Viscous Flow Computations for the Diffuser Section of a Large Water Tunnel

Ahmet Yusuf GÜRKAN[a,1] , Çağatay Sabri KÖKSAL[a,1],
Çağrı AYDIN[a,1], Uğur Oral ÜNAL[a,1]
[a] *Istanbul Technical University*

Abstract. A new research project, involving the construction of a modern, large, closed-circuit depressurised high-speed water tunnel to support the detailed hydro-acoustic, hydrodynamic, cavitation and flow visualization based experimental campaigns, is to be completed this year in Istanbul Technical University. An extensive computational study was conducted to design mainly the most critical sections of the tunnel. The results of the simulations concerning the hydrodynamic properties of the contraction and test sections of the tunnel were previously presented in NAV2015 conference. The present paper covers the fundamental viscous flow computations focusing the design of the diffuser section of the tunnel. In order to discharge the flow from the test section with minimum energy loses, diffuser takes a critical place at the downstream side of the test section for water tunnels. Therefore, achievable minimum pressure loss is directly related with length scale of the flow separation region along the diffuser. Furthermore, this flow phenomenon directly affects the acoustical performance of the tunnel with decreasing overall back noise level as well as the flow uniformity in test section. The paper does not only cover the hydrodynamic results of a constant-expansion-angle diffuser section but involves the design of a diffuser with three-step expansion structure aiming no or minimum flow separation region. Incompressible Reynold-Averaged-Navier-Stokes computations were performed for the simulations. The effect of several design parameters, which includes the expansion ratio and length of the diffuser geometry, was investigated. The influence of the chamfered corners was also considered.

Keywords. Viscous flow, Diffuser design, Asymmetric diffuser, RANS

1. Introduction

Despite the fact that computational fluid mechanics has gained considerable progress especially in the last two decades, water tunnels still remain as a crucial tool for model tests and basic hydrodynamic research.

A new large and high-speed cavitation tunnel has recently been building to substantially expand its existing experimental potential of Naval Architecture and Marine Engineering Department of Istanbul Technical University. The state-of-the-art facility intended would provide a wide-range of detailed experimental investigations involving hydroacoustics, hydrodynamics, cavitation, flow visualisation, etc. As a result

[1] A.Y. GÜRKAN, Ç.S,.KÖKSAL, Ç. AYDIN, U.O. ÜNAL, Naval Architecture and Marine Engineering Faculty, Naval Architecture Department, Istanbul Technical University, Ayazağa Campus, Maslak, İstanbul, The Turket; E-mail: gurkanah@itu.edu.tr (A.Y. Gurkan), koksalcag@itu.edu.tr (C.S. Köksal), aydinca@itu.edu.tr (C. Aydin), ounal@itu.edu.tr (U.O.Ünal)

of the general evaluation of the basic requirements, the length (L_t), height (H) and beam (B) of the test section of the cavitation tunnel were determined to be 5, 1.2 and 1.5 meters respectively whilst the maximum attainable flow velocity in the test section is decided to be 15 m/s.

In this study, the results of fundamental viscous flow computations concerning mainly the design of the diffuser section of the new tunnel were presented. Several design parameters were analysed to obtain a final effective base geometry to be further optimised in the detailed design stage with the invaluable knowledge gained with these preliminary computations. The following paragraphs briefly present the mentioned computer simulations.

2. Geometry and Parametrisation

The main purpose of the diffuser is to reduce the speed of the flow exiting from the test section to the desired level. Consequently, the flow separation in the diffuser should be minimized or entirely avoided.

The expansion ratio (d) is a highly critical parameter for the diffuser design. It is simply defined as the ratio of cross-section areas of the diffuser's entrance and exit. This ratio mainly determines the flow speed entering the high-speed vaned-elbow and it also partly designates the dimension of the remaining parts up to the pump section.

Another parameter to be taken into consideration is the expansion angle (θ) of the diffuser to provide a flow without excessive energy losses and flow separation. In the study, side walls (θ_s) and floor expansion angle (θ_f) were controlled individually. The maximum expansion angle in the diffuser is recommended to be between 6° and 8° [1].

In the light of the information above, the expansion ratio (d) and the diffuser expansion angle (θ) were considered as the basic parameters to be investigated. As the length of diffuser (L_d) is strongly associated with the selected values of d and θ, it was also evaluated as a part of the systematic analyses. Considering the basic dimensions of the large, high-speed water tunnels, which are currently active in the science and engineering field [2], an expansion ratio within 3.0 and 4.0, was initially decided for the simulations. Due to the constructive and economic limitations, the maximum overall length of the cavitation tunnel was the primary constraint. Accordingly, by taking the predetermined dimensions of the contraction and test section [3] into consideration, a diffuser length of below 20 m was initially targeted.

The diffuser entrance was normally controlled by the height and beam dimensions of the test section, while an asymmetric square cross-section was adopted at exit of diffuser. Symmetrical or circular cross section shaped diffuser models are not included in this study.

3. Computational Study

3.1. Solution Method and Computational Model

The computations were carried out with the incompressible RANS equations. SST k-ω turbulence model [4] was used in the simulations, which is based on the Boussinesq hypothesis [5] and is considered as an improved version of the standard k-ω model [6].

A segregated algorithm was used in conjunction with the finite volume method [7] to solve the momentum and turbulent transport equations. The pressure-correction-based SIMPLE technique [8] was used to couple the pressure and velocity fields. The spatial discretization of the convective terms of the Navier-Stokes and turbulent transport equations was achieved with a second-order-upwind scheme [9] while a second-order central differencing scheme was used for the viscous terms.

A H-type structured fine mesh was created for the full-scale computational model. The positive Y axis side of the longitudinal symmetry plane was solely used in the computations. Non-dimensional wall distance values (y^+) of about 50 were selected for the majority of the computational domain, mainly, due to the hardware resource limitations, which involved the use of the wall functions.

Two computational models were basically considered. Whilst the basic model lacked the existence of the contraction, the extended one involved the three fundamental components which are the contraction, test and diffuser sections. Additionally, entrance and exit sections with a length of around L_t and L_d were added to the geometry in order to place the inlet and outlet boundaries at an adequate distance to avoid the potential numerical problems for both models.

Two origin locations were considered in the study. The first one was placed at the center of the longitudinal symmetry plane at the middle of the test section. The second origin location was used to present the plots associated with the diffuser. It was simply placed at the center of the entrance plane of the diffuser. The test section design velocity was selected to be 10 m/s. The velocity magnitudes of 2 and 15 m/s were also considered in the computational simulations.

3.2. Grid Dependence and Validation Study

Three different mesh models with different cell sizes were prepared for the grid dependence analysis. The grid size ratio of the meshes was set to ~1.3 and 1.9 in each axis direction. The average value of the grids' aspect ratios was lower than 20, for all mesh models. The grid dependence simulations were run at the design speed of 10 m/s. In each case, the iterations were run until the scaled residuals drop to 10^{-7}, and also minimum wall shear stress at flow direction reduces to 10^{-4}. In addition, after each iteration, the variation of the flow variables at various locations in the domain was inspected. The results of the pressure losses and the minimum friction coefficient ($C_{f,min}$) in the diffuser are collected in Table 1. As is seen, the differences of the results obtained from the mesh B and C are notably low. Thus, an adequate accuracy was found to be obtained with the mesh B and the rest of simulations were conducted with this mesh resolution.

Since diffusers contain strong adverse pressure gradients, severe flow separation zones can also exist inside them. Therefore, an accurate detection of these zones in the computational simulations is a highly critical issue and a fundamental step of the design stage. The validation case was carried out with 2D asymmetric diffuser model which has both experimental and computational results with different turbulence models [10], [11].

Table 1. Grid dependence analysis - basic flow parameters

Mesh	Cell count	Pressure losses (Pa)	Diff. %	$C_{f,min}$	Diff. %
A	977,600	10.2	10.2	-0.829	5.9
B	3,391,200	6.32	6.32	-0.789	0.8
C	6,916,000	5.7	0.326	-0.783	-

A Reynolds number (Re) of 18,000 was considered for the validation case. The computational domain was formed according to the geometry given in [14]. A high-quality mesh structure with an adequate resolution was generated in the light of the grid dependence study performed. The comparative results of the pressure coefficients, on the other hand, can be seen in Figure 1. As clearly seen, the agreement with the experimental data is very good. Table 2 collects the results for the location of the separation inception and reattachment comparison with different studies.

The comparison the CFD results of experiment and literature is gathered in Table 2. The case result and its set up setting is accurate according to experiment result.

Moreover, the pressure coefficient distribution of the study was in agreement with the experiment data, so subsequent simulations was conducted with this case.

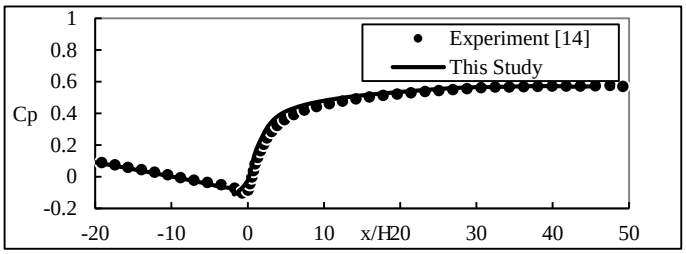

Figure 1. Comparative pressure coefficients on lower wall.

Table 2. Validation analyses - comparison

	Experiment [14]	**CFD [11]**	**This study**
Separation (x/H)	7.4	2.2	4.8
Reattachment (x/H)	29.2	30.2	28.3

4. Results and Discussion

The pressure loss (ΔP) caused by the diffuser can be easily calculated according to the energy balance equation as follows:

$$\Delta P = (\overline{P_1} + 1/2 \rho \overline{U_1}^2) - (\overline{P_2} + 1/2 \rho \overline{U_2}^2) \quad (1)$$

where $\overline{P}_1$, $\overline{U}_1$, $\overline{P}_2$ and $\overline{U}_2$ represent the average pressure and streamwise velocity values, respectively, at the diffuser entrance and exit. The hydrostatic pressure was excluded in Equation 1. Non-dimensional representation by means of the pressure loss coefficient can also be calculated by using the dynamic pressure in the test section.

Additionally, since zero x-shear stress (τ_X) represents flow separation inception, distribution of τ_X in the streamwise (X axis) direction was decided to take reference to eliminate flow separation with changing ratio of cross section area along the diffuser.

To compare separation zones characteristics between the cases with different diffuser length, the separation inception location (x_i) from the diffuser entrance and the separation zone length was divided to the diffuser length (L_d) so as to create a non-dimensional separation length (L_S) value.

The first studies were performed with a flat-top asymmetric geometry with constant expansion angles of the bottom and side walls along the diffuser. The design velocity of 10 m/s, which corresponded to a Reynolds number (Re) of 1.2 x 10^7 based on test section height (H), were used in the computations. Several cases with the basic computational model, which does not include the contraction geometry, were performed with different diffuser length and expansion ratios within a wide range of L_d =20-26 m and d=3.0-3.5. The results are given in Table 3.

Table 3. Cases with constant expansion angle.

Case	d	L_d (m)	Expansion Angle θ_f	θ_S	x_i (m) Floor	x_i (m) Ceiling	τ_x (min) (Pa) Floor	τ_x (min) (Pa) Ceiling	L_S/L_d	K e-2
1	3.0	22	2.9	1.1	8.261	9.790	-0.527	-0.251	0.632	7.1
2	3.0	24	2.7	1.0	10.728	12.120	-0.505	-0.195	0.557	9.5
3	3.0	26	2.5	0.9	12.038	14.560	-0.302	-0.179	0.535	7.3
4	3.5	20	3.7	1.4	4.140	5.301	-1.455	-0.416	0.878	8.1
5	3.5	22	3.4	1.3	5.170	6.534	-0.995	-0.380	0.820	7.7
6	3.5	24	3.1	1.2	6.384	7.944	-0.705	-0.320	0.791	7.5

Minimum loss coefficient (K) among the diffusers with constant expansion angle was calculated as 0.073 for the Case-3, due the its relatively small separation zone generated.

Based on the results of the initial simulations, it was clear that it was almost impossible to obtain an entirely separation-free flow field in the diffuser by using constant θ values within the design limitations. Accordingly, the subsequent simulations were carried out with a stepped geometry which includes three equal-length parts with varying θ values. In this way, a more effective control on the pressure gradient inside the diffuser and wall shear stresses was intended. Basically, three different expansion angle combinations were applied with increasing/decreasing bottom/side wall(s) angles along the diffuser. Additionally, in order to further improve the diffuser geometry, a flat chamfer with a thickness of 5 cm was applied to the floor and ceiling corners where the flow separation was expected to occur.

The general character of the skin friction coefficient values computed on the floor and ceiling surfaces along the symmetry plane are shown in Figure 2. The basic properties of the cases presented in the figure are collected in Table 4.

According to C_f distribution along edges of diffuser, it was distinctly seen that most critical zone starts at the middle of diffuser. Therefore, it was found appropriate to dedicate most of the area increments at the first three-quarters of the diffuser. Thereby, Combination C investigated on diffuser expansion angles.

Table 4. Expansion angle combinations cases

Comb.	d	L_d [m]	θ_f st	θ_f nd	θ_f rd	θ_S st	θ_S nd	θ_S rd
A	3.0	18	2.6	3.5	4.6	0.9	1.2	1.8
B	3.0	18	2.6	3.5	4.6	1.8	1.2	0.9
C	3.0	18	4.6	3.5	2.6	0.9	1.2	1.8
D	3.0	18	4.6	3.5	2.6	1.8	1.2	0.9

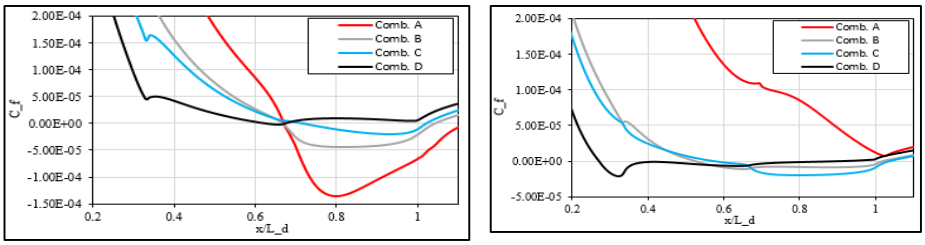

Figure 2. C_f distribution on diffuser for different combination.

The diffuser combination C was evaluated with different length scales. For initial calculation, first and third steps' angle were decided to offset around 20% of its related reference angle. Thus, the second angle was set as the reference angle.

As is seen in Table 5, for Case-9 and 10, the pressure drop caused by the viscous effects is more dominant than the friction loses. This implies that the separation size was reduced while the diffuser length was increased.

According to graph, Case-10 had separation inception point at 0.90 and 0.53 in diffuser on the floor and the ceiling corner respectively, it was decided to increase cross section area of the first half of the diffuser by controlling only the side walls' angle from wider angle to narrower. Although this approach resulted in success on the floor corner, flow separation was detected on the ceiling edges, while the pressure gradients and magnitude of C_f were reducing for Case-11. At next step, the cross-section area controlled via increasing the first angle of the floor wall while decreasing the side walls' angles. Hereby, Case-12 had no flow separation zones on the floor and ceiling edges with uniform velocity inlet where it was located 5 m before the test section entrance, without the contraction section. Finally, a diffuser geometry was developed with no separation zone. Figure 3 represents how Case-12 was improved step by step starting from Case-10 considering the adverse pressure gradient, separation point and length by controlling both sides and floor angles.

Table 5. Results of different diffuser geometry.

Case	d	L_d (m)	θ_f			θ_s			$\tau_{x\,min}$ (Pa)		L_s		K e-2
			st	nd	rd	st	nd	rd	Flr.	Clng	Flr	Clng	
7	3.0	18	4.6	3.5	2.6	0.9	1.2	1.8	-1.00	-0.93	0.322	0.457	6.6
8	3.0	20	3.6	3.2	2.9	1.3	1.2	1.0	-0.14	-0.25	0.084	0.429	6.3
9	3.0	18	3.9	3.6	3.2	1.4	1.3	1.2	-0.77	-0.05	0.640	0.498	6.4
10	3.0	19	4.2	3.4	2.6	1.2	1.2	1.2	-0.15	-0.31	0.905	0.526	6.2
11	3.0	19	4.2	3.4	2.6	1.8	1.1	0.8	-	-0.18	-	0.522	5.7
12	3.0	19	4.5	3.2	2.5	1.6	1.2	0.9	-	-	-	-	5.6

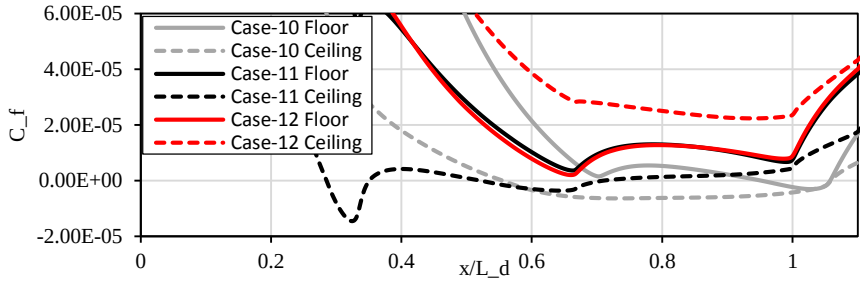

Figure 3. C_f distribution along diffuser edges

Table 6 shows that the Case-12* with the extended computation domain by adding the contraction geometry to flow volume changed result dramatically. Thereby, it was possible to compare how results affected with different velocity distributions at the entrance surface of the diffuser. The flow uniformity in a particular transverse cross-section of the test section can be expressed by the relative difference between the streamwise velocity at any point (outside the boundary layer) on this section and U_C. Accordingly,

$$FU_X(\%) = \frac{U_C - U_X}{U_C} \times 100 \qquad (3)$$

may be written for the percentage of the streamwise (X axis direction) flow uniformity at any particular cross-section. For the velocities in the Z directions, the U_C value in the numerator is ignored.

Flow velocity at x direction of Case-12 is faster than extended version on the test section floor. Furthermore, FU_Z is between -0.1 and -0.6 for flow volume without contraction geometry while extended model is between 0.3 to -0.3. As a result, strong flow separation had been observed in the diffuser at extended case.

In Table 7, the results associated with Case-13, 14 and 15 are collected, which were designed with a similar approach to that used in the previous cases involving no contraction section.

Table 6. Results of different diffuser geometry with contraction geometry.

Case	d	L_d (m)	θ_f			θ_s			$\tau_{x\,min}$ (Pa)		L_s		Ke-2
			st	nd	rd	st	nd	rd	Flr.	Clng	Flr	Clng	
12*	3.0	19	4.5	3.2	2.5	1.6	1.2	0.9	-5.9	-	0.273	-	7.4
13	3.0	19	2.5	3.2	4.5	1.6	1.2	0.9	-3.75		0.536	-	8.9
14	3.0	19	2.5	3.2	4.5	2.4	0.9	0.4	-1.49	-	0.622	-	7.6
15	2.8	19	2.7	3.1	3.7	2.4	0.9	0.1	-	-	-	-	6.6
16	2.8	19.5	2.5	3.0	3.7	2.3	0.9	0.1	-	-	-	-	7.2

In Table 6, it can be seen that Case-15 displays no trace of flow separation and provides a minimum pressure drop value. However, according to the results presented in Table 7, a flow separation was still apparent at a flow velocity of 2 m/s. Therefore, the diffuser length was increased up to 19.5 m and the expansion ratio was reduced to 2.8 to overcome this undesired flow phenomenon (Case-16). However, although the separation level relatively was reduced, it could not be eliminated completely.

Table 7. Different velocity inlet conditions results.

Case	U (m/s)	θ_f			θ_s			$\tau_{x\,min}$ (Pa)		L_s		Ke-2
		st	nd	rd	st	nd	rd	Flr.	Clng	Flr	Clng	
15	2	2.7	3.1	3.7	2.4	0.9	0.1	-0.28	-	0.748	-	8.9
16	2	2.5	3.0	3.7	2.3	0.9	0.1	-0.16	-	0.725	-	7.2
16	15	2.5	3.0	3.7	2.3	0.9	0.1	-	-	-	-	8.7

Flow uniformity in all three direction and the turbulence ıntensity is at the desired level, less than ±1% and 1% respectively in the test section.

Comparing the results obtained here with the results with no diffuser geometry [3], it is possible to observe the positive contribution of the diffuser geometry to the flow quality in the test section, and particularly to the turbulence intensity.

5. Conclusions

Full-scale viscous flow computations were performed for the diffuser geometry of the high-speed, large cavitation tunnel of Istanbul Technical University, which is to be constructed as a part of a research project.

A three-step expansion approach for the diffuser floor and side walls was adopted for the design process. Simulations with three different flow velocities and several diffuser expansion ratios and angles were carried out.

The separation region in the diffuser was directly affected from the existence of the contraction, which changed the velocity distribution particularly in vertical direction at the diffuser entrance. The simulations with constant expansion angle displayed clear separation zones. Thus, the study proceeded with a three-step diffuser geometry. The location of the separation inception and separation length was controlled by separately adjusting the diffuser floor and side angles. The combination of increasing the step angles of the diffuser floor and decreasing those of the sides walls provided an adequate diffuser length and a minimum pressure drop level. The application of chamfered edges further improved the results by decreasing both pressure drop and size of separation length. The turbulence intensity was also significantly reduced in the middle plane of the test section with the existence of the diffuser.

References

[1] J.F. Ripken, *Design Studies For A Closed-Jet Water Tunnel. Minneapolis*, Minnesota, St.Anthony Falls Hydrolic Laboratuary, USA: University of Minnesota, 1951.

[2] D.B. Gleed, and G. Saiva, *A Selective Survey Of Literature on Water Tunnels To Provide A Basis*. Lucas Heights: Australian Atomic Energy Commission, 1967.

[3] A.Y. Gürkan, G. Bilici, U.O. Ünal, *Viscous Flow Computations for a Large Water Tunnel*, 18th International Conference on Ships and Shipping Research, Lecco Italy, 2015

[4] F. R. Menter, Two-Equation Eddy-Viscosity Turbulence Models for Engineering Applications, *AIAA* Journal **32(8)** (1994), 1598-1605.

[5] H. Tennekes, and J. L. Lumley. *A First Course in Turbulence*, UK: MIT Press, Cambridge, 1972.

[6] D.C. Wilcox, Reassessment of The Scale-Determining Equation for Advanced Turbulence Models, *AIAA Journal* **26 (11)** (1988), 1299–1310.

[7] J. Blazek, *Computational Fluid Dynamics: Principles and Applications*, UK: Elsevier, Oxford, 2001.

[8] S.V. Patankar, and D.B. Spalding, A Calculation Procedure for Heat, Mass and Momentum Transfer in Three-Dimensional Parabolic Flows, *International Journal of Heat and Mass Transfer* **15** (1972), 1787-1806.

[9] L. Davidson, *Numerical Methods for Turbulent Flow, MTF071 Lecture Notes*, Chalmers University of Technology, Göteborg, Sweden: Department of Thermo and Fluid Dynamics, 2005.

[10] C.U. Buice, and J.K. Eaton.. Experimental investigation of flow through an asymmetric plane diffuser, *J. Fluids Eng.* **122:433–5** (2000).

[11] S.M. El-Behery, and M.H. Hamed.. A comparative study of turbulence models performance for separating flow in a planar asymmetric diffuser, *Computers & Fluids* (2011), 248–257.